



# Studies of tricyclic piperazine/piperidine furnished molecules as novel integrin $\alpha_v\beta_3/\alpha_{IIb}\beta_3$ dual antagonists using 3D-QSAR and molecular docking

Yulian Yan<sup>a</sup>, Yan Li<sup>a,\*</sup>, Shuwei Zhang<sup>a</sup>, Chunzhi Ai<sup>b</sup>

<sup>a</sup> School of Chemical Engineering, Dalian University of Technology, Dalian, 116012, Liaoning, China

<sup>b</sup> Lab of Pharmaceutical Resource Discovery, Dalian Institute of Chemical Physics, Graduate School of the Chinese Academy of Sciences, Dalian, 116023, Liaoning, China

## ARTICLE INFO

### Article history:

Received 30 July 2010

Received in revised form

10 December 2010

Accepted 20 December 2010

Available online 8 January 2011

### Keywords:

3D-QSAR

Integrin  $\alpha_v\beta_3$

Integrin  $\alpha_{IIb}\beta_3$

Antagonist

CoMFA

CoMSIA

## ABSTRACT

The development of injectable integrin  $\alpha_v\beta_3/\alpha_{IIb}\beta_3$  dual antagonists attracts much attention of research for treating of acute ischemic diseases in recent years. In this work, based on a dataset composed of 102 tricyclic piperazine/piperidine furnished dual  $\alpha_v\beta_3$  and  $\alpha_{IIb}\beta_3$  antagonists, a variety of *in silico* modeling approaches including the comparative molecular field analysis (CoMFA), comparative similarity indices analysis (CoMSIA), and molecular docking were applied to reveal the requisite 3D structural features impacting the biological activities. Our statistical results show that the ligand-based 3D-QSAR models for both the  $\alpha_v\beta_3$  and  $\alpha_{IIb}\beta_3$  studies exhibited satisfactory internal and external predictability, i.e., for the CoMFA models, results of  $Q^2 = 0.48$ ,  $R^2_{ncv} = 0.87$ ,  $R^2_{pred} = 0.71$  for  $\alpha_v\beta_3$  and  $Q^2 = 0.50$ ,  $R^2_{ncv} = 0.85$ ,  $R^2_{pred} = 0.72$  for  $\alpha_{IIb}\beta_3$  analysis were obtained, and for the CoMSIA ones, the outcomes of  $Q^2 = 0.55$ ,  $R^2_{ncv} = 0.90$ ,  $R^2_{pred} = 0.72$  for  $\alpha_v\beta_3$  and  $Q^2 = 0.52$ ,  $R^2_{ncv} = 0.88$ ,  $R^2_{pred} = 0.74$  for  $\alpha_{IIb}\beta_3$  were achieved respectively. In addition, through a comparison between 3D-QSAR contour maps and docking results, it is revealed that the most crucial interactions occurring between the tricyclic piperazine/piperidine derivatives and  $\alpha_v\beta_3/\alpha_{IIb}\beta_3$  receptor ligand binding pocket are H-bonding, and the key amino acids impacting the interactions are Arg214, Asn215, Ser123, and Lys253 for  $\alpha_v\beta_3$ , but Arg214, Asn215, Ser123 and Tyr190 for  $\alpha_{IIb}\beta_3$  receptors, respectively. Halogen-containing groups at position 15 and 16, benzene sulfonamide substituent at position 23, and the replacement of piperazine with 4-aminopiperidine of ring B may increase the  $\alpha_v\beta_3/\alpha_{IIb}\beta_3$  antagonistic activity. The potencies for antagonists to inhibit isolated  $\alpha_v\beta_3$  and  $\alpha_{IIb}\beta_3$  are linear correlated, indicating that similar interaction mechanisms may exist for the series of molecules. To our best knowledge this is the first report on 3D-QSAR modeling of these dual  $\alpha_v\beta_3/\alpha_{IIb}\beta_3$  antagonists. The results obtained should provide information for better understanding of the mechanism of antagonism and thus be helpful in design of novel potent dual  $\alpha_v\beta_3/\alpha_{IIb}\beta_3$  antagonists.

© 2011 Elsevier Inc. All rights reserved.

## 1. Introduction

Blood platelets are irregularly-shaped, colorless bodies that are present in blood with essential roles in normal coagulation as well as some diseases such as coronary atherosclerosis [1]. Currently, the utility of anti-platelet therapies in the management of the platelet-associated disease states further emphasizes the pivotal role the platelets play in the pathogenesis of cardiovascular disease [2].

In the last several decades, a family of adhesion receptors known as integrin receptors which recognize an Arg-Gly-Asp (RGD) tripeptide [3,4] has been reported to be related to coagulation blood platelets. As also a family of cell surface heterodimeric adhesion

receptors, these integrins consist of  $\alpha$  and  $\beta$  chains [5], linking the cytoskeleton to the extracellular matrix and regulating key signaling events that coordinate the cellular processes such as secretion, migration, and proliferation [6].

The integrin  $\alpha_v\beta_3$  is expressed as a major surface molecule on endothelial cells described as the vitronectin receptor [7]. Since it is found being implicated in various physiological and pathological processes such as the migration of smooth muscle cells, angiogenesis, tumor metastasis, neointimal hyperplasia, metabolism of the bone and arterial restenosis [8],  $\alpha_v\beta_3$  is considered as a potential drug target, and several groups are searching for orally active, small-molecular antagonists as candidate drugs to treat related diseases including the arterial thrombosis [9,10]. Therefore, numerous studies are carried out in developing integrin  $\alpha_v\beta_3$  antagonists as injectable drugs, due to the association of  $\alpha_v\beta_3$  with the adhesion and migration of vascular smooth muscle cells and leukocytes.

\* Corresponding author. Tel.: +86 411 84986062; fax: +86 411 84986063.

E-mail address: [yanli@dlut.edu.cn](mailto:yanli@dlut.edu.cn) (Y. Li).

Moreover, integrin  $\alpha_v\beta_3$  binds to a variety of RGD containing adhesive proteins such as the vitronectin, fibronectin, von Willebrand factor (vWF), fibrinogen, osteopontin, bone sialo protein II, and thrombospondin [11]. The related integrin  $\alpha_{IIb}\beta_3$  also interacts through this mechanism and the antagonists of  $\alpha_{IIb}\beta_3$ , particularly the RGD peptides and small-molecule RGD peptidomimetics, have received considerable attention [12]. Therefore, it is very promising for injectable  $\alpha_v\beta_3/\alpha_{IIb}\beta_3$  dual antagonists to be candidate drugs for curing the acute ischemic disease, where the Fab fragment of the human-murine monoclonal antibody Abciximab is already in use [13].

The related integrin  $\alpha_{IIb}\beta_3$  which has narrow expression compared with  $\alpha_v\beta_3$  restricted to platelets and megakaryocytes [8], serves as the receptor for fibrinogen and other adhesive proteins, after platelet activation by a variety of agonists generated or exposed upon vascular lesion, and plays a primary role in platelet aggregation, platelet spreading on the exposed subendothelium, and clot retraction [14].  $\alpha_{IIb}\beta_3$  is inactive in unstimulated platelets. Whereas when following the platelet stimulation by certain agonists like thrombin,  $\alpha_{IIb}\beta_3$  assumes a conformation capable of binding macromolecular ligands (e.g. fibrinogen) [15]. Up to now, there are altogether four classes of  $\alpha_{IIb}\beta_3$  antagonists, including the monoclonal antibodies (7E3 [13]), polypeptides containing an RGD or KGD sequence isolated from snake venoms or leeches (decorsin [16]), low molecular weight linear or cyclic peptides containing either an RGD sequence or the carboxyl terminal sequence of the  $\gamma$ -chain of fibrinogen (eptifibatide [17]), and peptidomimetics or non-peptide antagonists (tirofiban, sibrafiban, and lamifiban) [17].

Therefore, extensive ligand-based drug design studies, using cyclic peptide libraries with constrained backbone conformations, led to the discovery of the  $\alpha_v\beta_3$ -selective first generation cyclic pentapeptide cyclo(-RGDFV-). The systematic derivatization of this peptide resulted in the N-alkylated cyclopeptide cyclo(-RGDF[NMe]V-) [18], which is already in clinical phase as anti-cancer drug (Cilengitide, EMD121974) now. Thereafter, extensive development of  $\alpha_v\beta_3$  antagonists was reported [19], where some dual  $\alpha_v\beta_3/\alpha_{IIb}\beta_3$  antagonists attracted more interests of research. SmithKline Beecham (SB; King of Prussia, PA, USA) extended the initial observations to the small-molecule area with the identification of SB223245 [20], a potent  $\alpha_v\beta_3$  antagonist with good selectivity over  $\alpha_{IIb}\beta_3$ . Another dual  $\alpha_v\beta_3/\alpha_{IIb}\beta_3$  antagonist was reported by Scripps (La Jolla, CA, USA) describing a series of derivatives closely related to the Merck compound L748415. Moreover, DuPont lately reported the identification [21] and detailed characterization process of SM256, another promising antagonist, which not only exhibits modest selectivity for  $\alpha_v\beta_3$  over  $\alpha_{IIb}\beta_3$ , but also possesses high selectivity over  $\alpha_v\beta_5$  which is another related integrin.

Though only having as young as 22 years of history as proposed in 1988 in term of the comparative molecular field analysis (CoMFA) method by Crammer et al, the three-dimensional quantitative structure-activity relationship (3D-QSAR) approaches have been extensively used in many present practices of drug discovery and development [22], due to their outstanding advantages of time-saving, cost-reducing as well as the high efficiency in silico screening and prediction of candidate drugs.

In this paper, we focused on another series of mimetics of the RGD tripeptide sequence small-molecular antagonists, tricyclic piperazine/piperidine furnished molecules which were dual integrin  $\alpha_v\beta_3$  and  $\alpha_{IIb}\beta_3$  antagonists, with purpose to rationalize the molecular variations to their antagonistic activities. To this end, a total of 102 these noncompetitive antagonists were collected to build 3D-QSAR models, by combinational use of the CoMFA [22] and comparative molecular similarity indices analysis (CoMSIA) [23] 3D-QSAR methods. The predictive abilities of the obtained models were then checked and validated statistically with an inde-

pendent test set of compounds. Furthermore, a docking analysis was employed to elucidate the probable binding modes of these inhibitors at the allosteric site of the enzyme. To our best knowledge, this work provides the first 3D-QSAR study for dual  $\alpha_v\beta_3$  and  $\alpha_{IIb}\beta_3$  antagonists and the models established, we hope, would be of help for design of more potent tricyclic piperazine/piperidine based  $\alpha_v\beta_3$  and  $\alpha_{IIb}\beta_3$  antagonists.

## 2. Materials and methods

### 2.1. Dataset and biological activity

Discarding those compounds with unspecified antagonistic activity and the chemicals with undefined stereochemistry, a total of 102 tricyclic piperazine or piperidine furnished molecules with a wide spectrum of antiplatelet activities against dual  $\alpha_v\beta_3$  and  $\alpha_{IIb}\beta_3$  receptors were collected from the work of D. Kubota et al. and used as the dataset for molecular modeling in this study [2,10,24,25]. In this work, the in vitro biological activities of these compounds were converted into the corresponding  $pIC_{50}$  ( $-\log IC_{50}$ ) values, which were used as dependent variables in the QSAR analyses. In approximately a ratio of 4:1 the whole data set was divided into training (81) and test (21 molecules) sets, respectively. All structures and the binding affinity  $IC_{50}$  values of the dataset against both the  $\alpha_v\beta_3$  and  $\alpha_{IIb}\beta_3$  receptors, as well as their belongings to the training or test set are listed in Tables S1–S16 (Supporting Information). The principle for selection of the test set chemicals was to ensure that, on one hand, their  $pIC_{50}$  values are randomly but uniformly distributed in the range of the values for the whole set, and on the other hand, their structures cover as large diversity as possible of the dataset so that the derived models could represent the real characteristics of all the compounds both from the biological activity and the structures. Specifically, this selection is basically based on the distribution of the antagonist activity. As shown in Fig. 2, the molecules in the test set were selected manually such that: (1) the low, moderate, and high activity compounds were present approximately equal proportions in both sets; (2) the activity scale of the training set covers that of the test one.

In addition, the selection also took consideration of the structural diversity of the molecules. Based on the skeleton structure, the antagonists can be divided into 16 classes as shown in Tables S1–S16 of supporting information. The final molecules selected as the test set one were also almost proportioned to and located in every class. To illustrate this, a principal component analysis (PCA) was performed on the dataset as follows: (1) a total of 615 structural descriptors including the topological, constitutional, walk and path counts, atom-centred fragments and connectivity indices for each molecule were calculated for all the compounds using Dragon software [26]; (2) PCA was then performed within the calculated structure descriptors space for the whole data set, giving three significant principal components (PCs) which explains totally 73.39% of the variation in the data (58.35%, 9.39%, and 5.65%, respectively). Fig. S1 (supporting information) shows the distribution of the compounds over the three PCs. It can be seen clearly that the majority of the test set molecules were distributed due to the structure deviation among these compounds [27–31]. Table 1 depicts some representative skeletons and  $IC_{50}$  values (nM) of the dataset.

All molecular modeling and 3D-QSAR studies were performed using the SYBYL6.9 molecular modeling software package (Tripos Associates, St. Louis, MO). Partial atomic charges were calculated by the Gasteiger-Huckel method [32], energy minimization and conformational search were performed using Tripos molecular mechanics force field [33] by conjugating method with a convergence criterion of 0.001 kcal/mol. To obtain the most stable conformation, the energy gradient limit was set at 0.05 kcal/molÅ.

**Table 1**  
Representative structures and antagonistic activities of the dataset.

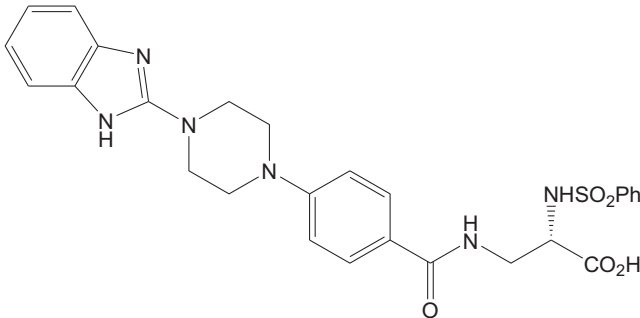
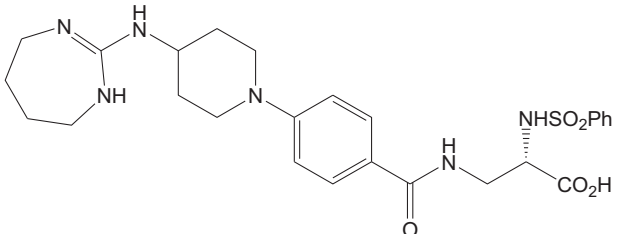
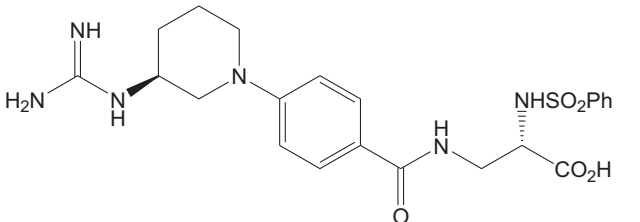
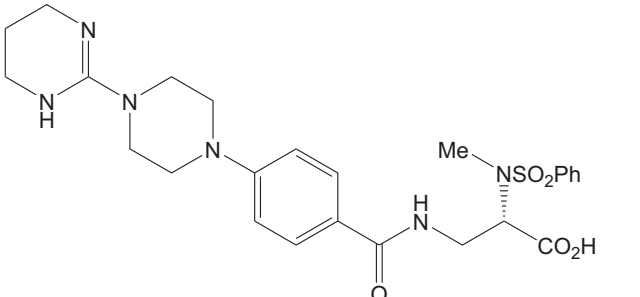
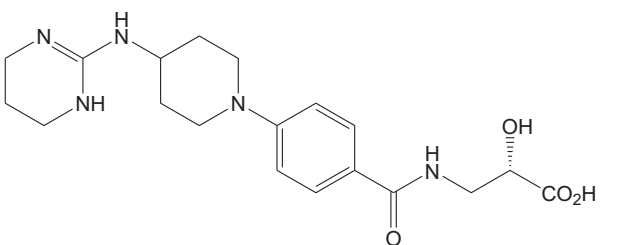
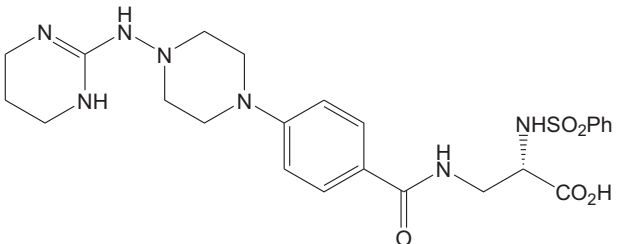
NO	Compound	Structure	IC <sub>50</sub> (nM)	
			$\alpha_v\beta_3$	$\alpha_{IIb}\beta_3$
4	16A		64	1.2
8	18B		0.59	0.21
12	33C		1.5	0.29
16	27A		14,000	77
26	36B		17	9.8
35	47A		1.3	3.1

Table 1 (Continued)

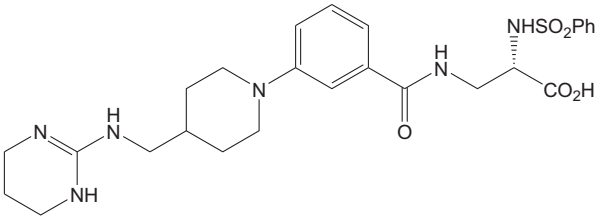
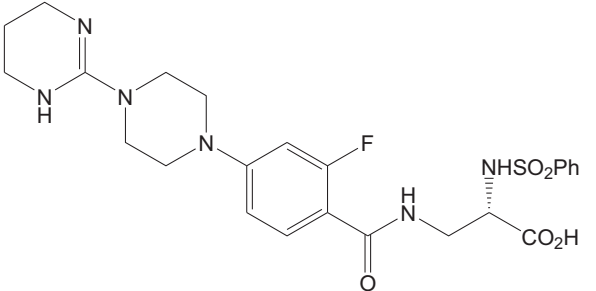
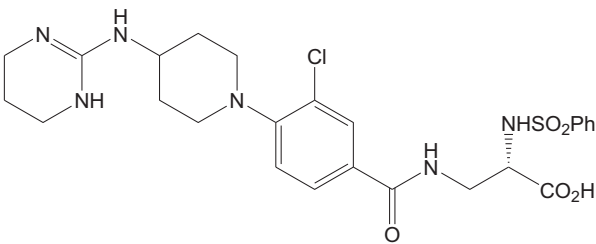
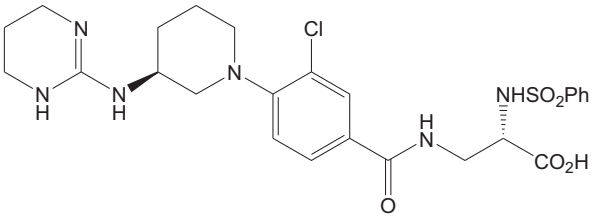
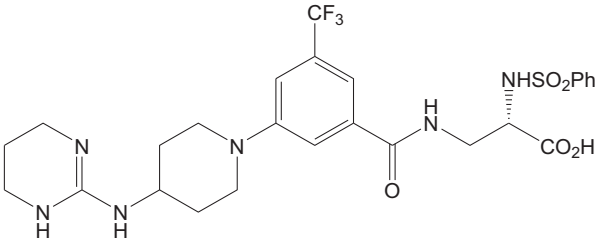
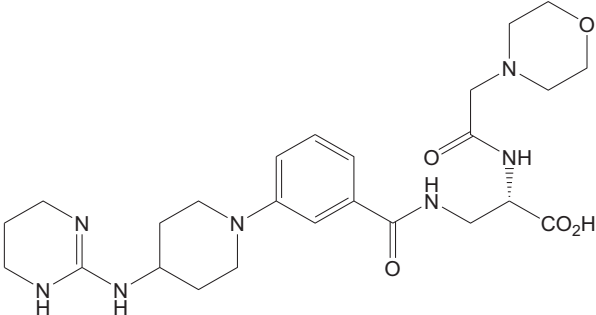
NO	Compound	Structure	IC <sub>50</sub> (nM)	
			$\alpha_v\beta_3$	$\alpha_{IIb}\beta_3$
45	31D		1,500	61
53	38A		31	0.41
58	9B		0.17	0.023
63	12C		3.2	0.34
72	47D		18	2,000
74	39D		17,000	1,300

Table 1 (Continued)

NO	Compound	Structure	IC <sub>50</sub> (nM)	
			$\alpha_v\beta_3$	$\alpha_{IIb}\beta_3$
80	44B		0.13	0.35
89	52B		0.14	0.18
92	10C		0.48	0.56
101	24A		7,000	10,000

## 2.2. Conformational sampling and alignment

Molecular alignment of compounds is a crucial step in the development of 3D-QSAR models [34]. It was assumed that each molecule binds into the integrin active site in a similar mode, since the compounds share a common scaffold. To derive the best possible 3D-QSAR statistical model, two different alignment rules were adopted. Initially, the ligand-based alignment rule was adopted. During the process, the most potent dual antagonist (compound 10B) was chosen as a template to fit the remaining training and test set of compounds by using substructure-alignment function available in SYBYL. Fig. 1A describes the common substructure for the alignment which is marked in bold. However, due to with no such substructure of Fig. 1A in the structures, compounds 23A, 24A and 25A were aligned based on another common substructure depicted in bold as shown in Fig. 1B. After the alignment, all molecules were

put into the same database. Fig. 1C shows the resulting ligand-based alignment model.

## 2.3. CoMFA and CoMSIA field calculation

The CoMFA and CoMSIA models were generated by using SYBYL 6.9 with the default parameters. Detailed algorithms of CoMFA and CoMSIA can be easily referred to many literatures, thus we only introduce the modeling parameters in this work.

To derive the CoMFA and CoMSIA descriptor fields, a 3D cubic lattice with grid spacing of 2 Å in x, y, and z directions, was generated automatically to encompass the aligned molecules. In CoMFA, the steric and electrostatic fields were calculated separately for each molecule using sp<sup>3</sup> carbon atom probe with a charge of +1.00 (default probe atom in SYBYL) and energy cut-off values of 30 kcal/mol for both the steric and electro-

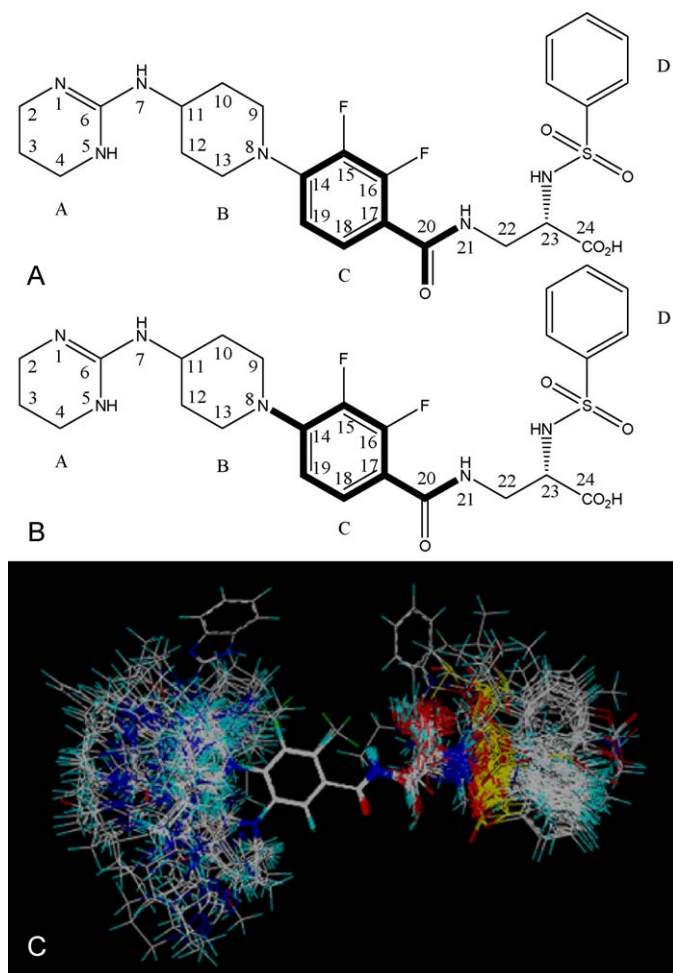


**Fig. 1.** The ligand-based alignment of all molecules in the dataset. Compound 10B is used as the template. (A) The common substructure (shown in bold) for the alignment of all molecules except 23A, 24A and 25A. (B) The common substructure (shown in bold) for the alignment of molecules 23A, 24A and 25A. (C) Ligand-based alignments of all the compounds as shown in panels. Molecules are colored in white for common C, blue for N, red for O, yellow for S, cyan for H, respectively. (For interpretation of the color information in this figure legend, the reader is referred to the web version of the article.)

static fields. The probe atom was placed at each lattice point, and their steric and electrostatic interactions with each atom in the molecule were computed using the CoMFA standard scaling.

CoMSIA similarity index descriptors were derived using the same lattice boxes as those used in CoMFA calculations. In CoMSIA, the steric, electrostatic, hydrophobic, and hydrogen-bond (H-bond) donor and acceptor descriptors were calculated using a probe atom of radius 1.0 Å, charge +1.0, and hydrophobicity +1.0. A Gaussian function is used to evaluate the mutual distance between the probe atom and each molecule atom. Because of the different shape of the Gaussian function, CoMSIA similarity indices ( $A_F$ ) for molecule  $j$  with atom  $i$  at grid point  $q$  are calculated by equation

$$A_{F,k}^q(j) = - \sum \omega_{\text{probe},k} \omega_{ik} e^{-\alpha r_{iq}^2} \quad (1)$$

where  $k$  represents the steric, electrostatic, hydrophobic, or hydrogen-bond donor or acceptor descriptor.  $\omega_{\text{probe},k}$  is the probe atom with radius 1.0 Å, charge +1, hydrophobicity +1, H-bond donating +1, H-bond accepting +1;  $\omega_{ik}$  is the actual value of the physicochemical property  $k$  of atom  $i$ ;  $r_{iq}$  is the mutual distance

between the probe atom at grid point  $q$  and atom  $i$  of the test molecule. The attenuation factor  $\alpha$  was set to 0.3.

#### 2.4. 3D-QSAR models calculation and validation

In order to generate statistically significant 3D-QSAR models, partial least squares (PLS) regression was used to analyze the training set by correlating the variation in their  $\text{pIC}_{50}$  values (the dependent variable) with variations in their CoMFA/CoMSIA interaction fields (the independent variables). PLS is a statistical approach that generalizes and combines features from principal component analysis and multiple regressions. It is particularly useful to predict a set of dependent variables from a large set of independent variables, and when the matrix of predictors has more variables than observations (multicollinearity).

To evaluate the reliability of the models generated from the PLS analysis, cross-validation analysis was accomplished with the leave-one-out (LOO) methodology wherein one compound was moved away from the dataset and its activity was predicted by the model derived from the rest of the dataset. A cross-validated correlation coefficient,  $Q^2$ , was subsequently obtained and provided as a statistical index of the predictive power. Then, a non-cross-validation analysis was carried out, the Pearson coefficient ( $R_{\text{ncv}}^2$ ) and standard error of estimates (SEE) were calculated. Finally, the CoMFA/CoMSIA results were graphically represented by field contour maps, where the coefficients were generated using the field type "Stdev\*Coeff".

In order to evaluate the real predictive ability of the best models generated by the CoMFA/CoMSIA analyses using the training set, the  $\text{pIC}_{50}$  values of 20 compounds are treated as the external validation set. A predictive  $R$  value was then obtained with the following formula:

$$R = \sqrt{\frac{\text{SD} - \text{PRESS}}{\text{SD}}} \quad (2)$$

where SD denotes the sum of squared deviation between the biological activities of the test set molecule and the mean activity of the training set molecules, PRESS represents the sum of squared deviations between the experimental and predicted activities of the test molecules.

#### 2.5. Molecular docking

To determine the probable binding conformations and offer more insight into the understanding of the interactions of integrins  $\alpha_v\beta_3$  and  $\alpha_{\text{IIb}}\beta_3$  receptor-antagonist, molecular docking analysis was carried out using the Surflex in SYBYL. The crystal structures of integrin  $\alpha_v\beta_3$  (3IJE) and  $\alpha_{\text{IIb}}\beta_3$  (2VDM) with inhibitors were collected from Brookhaven Protein Databank (PDB). This docking approach aligns the ligand to a "protomol" or idealized ligand in the active site of the target. Our molecular docking executes as the following steps: Firstly, the template protein structure obtained from the PDB databank was imported into Surflex. Then the protomol was generated using a ligand-based approach for integrin  $\alpha_{\text{IIb}}\beta_3$  (2VDM) and a residues-based approach for integrin  $\alpha_v\beta_3$  (3IJE). During the protomol generating process, the specification of two parameters is critical for forming appropriate binding pocket, in which one is the protomol.bloat determining how far from a potential ligand the site should extend, and the other is the protomol.threshold determining how deep into the protein the atomic probes used to define the protomol can penetrate. In the present work, for both the  $\alpha_v\beta_3$  (3IJE) and  $\alpha_{\text{IIb}}\beta_3$  (2VDM) docking analyses, the protomol.bloat value was set as 0 and the protomol.threshold value as 0.5 when a reasonable binding pocket was obtained. Finally, all the antagonists were docked into the binding pocket



**Table 2**  
CoMFA and CoMSIA results for integrin  $\alpha_v\beta_3/\alpha_{IIb}\beta_3$ .

PLS statistics	$\alpha_v\beta_3$		$\alpha_{IIb}\beta_3$	
	CoMFA	CoMSIA	CoMFA	CoMSIA
$Q^2$	0.48	0.55	0.50	0.52
$R^2_{ncv}$	0.87	0.90	0.85	0.88
SEE	0.59	0.51	0.52	0.45
$F$	103.61	178.91	104.39	135.14
$R^2_{pred}$	0.71	0.72	0.72	0.74
SEP	0.84	0.83	0.65	0.62
PLS components	5	4	4	4
Contribution				
Steric	0.63	0.15	0.58	0.17
Electrostatic	0.37	0.15	0.42	0.16
Hydrophobic		0.17		0.20
Hydrogen-bond donor		0.36		0.29
Hydrogen-bond acceptor		0.17		0.18

$Q^2$ , Cross-validated correlation coefficient after the leave-one-out procedure.  $R^2_{ncv}$ , non-cross-validated correlation coefficient. SEE, standard error of estimate.  $F$ , ratio of  $R^2_{ncv}$  explained to unexplained  $R^2_{ncv}/(1 - R^2_{ncv})$ .  $R^2_{pred}$ , predicted correlation coefficient for the test set of compounds. SEP, standard error of prediction. PLS components, optimal number of principal components.

and each of them had 10 conformations for  $\alpha_{IIb}\beta_3$  but 25 different conformations for  $\alpha_v\beta_3$ . During the docking process, the protein was considered as rigid and the antagonist molecules flexible. All other parameters were adopted default values.

The earliest identification of the ligand sites was achieved using the platelet integrin  $\alpha_{IIb}\beta_3$  [35] by several naturally occurring mutations in the  $\beta_3$  subunit which cause a severe bleeding disorder [36]. Recently, Springer TA et al. reported a crystal structure (PDB 2VDM) of integrin  $\alpha_{IIb}\beta_3$  headpiece bound to antagonist Tirfiban [37]. The active site was located in the aligend region. Previous cross-linking studies with RGD ligands using either  $\alpha_{IIb}\beta_3$  or  $\alpha_v\beta_3$  integrins not only established that the  $\beta$  and  $\alpha$  subunits had to be in close proximity for binding, but also defined the regions of binding in each subunit [38,39]. Therefore, the active sites were considered to be the  $\alpha_v\beta_3$  receptor's binding sites [40].

### 3. Results and discussion

To judge whether a QSAR model is reliable fitting for prediction of unknown molecules, several statistical parameters including especially the cross-validated correlation coefficient ( $Q^2$ ), non-cross-validated correlation coefficient ( $R^2_{ncv}$ ), and standard error of estimate (SEE),  $F$ -statistic values as well as the optimum number of components (OPN) should be evaluated. For both the  $\alpha_v\beta_3$  and  $\alpha_{IIb}\beta_3$  receptor 3D-QSAR studies, good correlations were observed in the obtained CoMFA and CoMSIA models demonstrated by the high values of  $Q^2$  and other statistical results. Table 2 summarizes the statistical results of the CoMFA and CoMSIA analyses.

#### 3.1. 3D-QSAR statistical results for integrin $\alpha_v\beta_3$

During the molecular modeling process for integrin  $\alpha_v\beta_3$ , 81 compounds out of the total 102 integrin  $\alpha_v\beta_3$  antagonists were used as training set and the remaining 20 compounds (compound 28C with no defined  $\alpha_v\beta_3$  experimental activity was discarded) were used as test set (shown as supporting Tables S1–S16).

For CoMFA analysis, the optimal model employing the steric and electrostatic field descriptors obtains a LOO cross-validated  $Q^2$  of 0.48 with 5 components, indicating a proper internal predictive capacity of the model. A high correlation coefficient ( $R^2$ ) of 0.87 for the non-cross-validated final model shows its self consistency. In addition, other statistical results including a SEE value of 0.59 and an  $F$ -test value of 103.61 all suggest that the CoMFA model is

a reliable predictor. In term of the relative contributions, the steric field accounts for 0.63, while the electrostatic field contributes 0.37, indicating that the steric property contributes a majority to the  $\alpha_v\beta_3$  antagonist activity.

For the CoMSIA analysis, all combinations of the five different field descriptors (the steric, electrostatic, hydrophobic, and H-bond-donor and H-bond-acceptor) were used, with attempt to, on one hand, seek for the best CoMSIA model, and on the other hand, avoid the risk of possibly omitting some of the optimal ones. As a result, out of all CoMSIA models established using the same training set as used in the CoMFA analysis, the optimal CoMSIA model made use of all five field parameters, and ended in statistical results of  $Q^2 = 0.55$ ,  $R^2_{ncv} = 0.90$ ,  $SEE = 0.51$ , and  $F = 178.91$  with 4 optimum components. Once again, the steric and electrostatic fields were demonstrated contributing a lot to the model (with a sum of 0.3 contribution) seen from Table 2. But at this time, the hydrogen bond descriptors including both the donor and acceptor fields outstand their roles for correlation with the  $\alpha_v\beta_3$  antagonist activity, where the former possesses 0.36 and the latter occupies 0.17 of relative contributions.

The test set of 20 antagonists was used to verify the efficacy of the CoMFA and CoMSIA models, when a predictive coefficient  $R^2_{pred}$  of 0.71 for CoMFA and 0.72 for CoMSIA were achieved, respectively (Table 2). Fig. 2A and B illustrate the correlation plots of the experimental versus the predicted  $pIC_{50}$  values of the training (filled black square) and test sets (filled blue circle) for the optimal CoMFA and CoMSIA models, respectively. Clearly, a good relationship was observed from this figure since the predicted values are almost as accurate as the experimental activities for the whole dataset, and all points are rather uniformly distributed around the regression line, indicating no existence of systematic errors in the method. This good agreement between the predicted and experimental activity data proves the satisfactory predictive ability of both the CoMFA and CoMSIA models.

#### 3.2. CoMFA and CoMSIA statistical results for integrin $\alpha_{IIb}\beta_3$

Discarding compound 36A whose  $\alpha_{IIb}\beta_3$  antagonist activity was not defined in the original experiment from the dataset, the remaining 101 antagonists were divided into a training set composed of 81 compounds and a test set consisting of 20 chemicals to derive the 3D-QSAR models (supporting Tables S1–S16).

For CoMFA analysis, the optimal model used both the steric and electrostatic field descriptors, and finally got a result of  $Q^2 = 0.50$ ,  $R^2_{ncv} = 0.85$ ,  $SEE = 0.52$ ,  $F = 104.39$  using 4 optimum components. Similar to the  $\alpha_v\beta_3$  CoMFA studies, the steric feature is found, again, making larger contribution (~58%) than the electrostatic one (~42%) to the  $\alpha_{IIb}\beta_3$  antagonist activity.

For CoMSIA analysis, the optimal model also calculated and employed the five fields of steric, electrostatic, hydrophobic, H-bond donor and acceptor interactions using the same probe atom as CoMFA analysis. And this model exhibits a proper internal predictivity demonstrated by the statistical results of  $Q^2 = 0.52$ ,  $R^2_{ncv} = 0.88$ ,  $SEE = 0.45$ ,  $F = 135.14$  based on the use of four optimum components. In this case, the steric and electrostatic fields also contribute a lot (with sum of 0.33) to the correlation with the activity. While similar to the CoMSIA model for  $\alpha_v\beta_3$  studies, the H-bond properties make the largest contribution (nearly 50%) to the activity, in which the contribution of H-bond donor (0.29) greatly outweighs the H-bond acceptor (0.18), indicating its vital role in stabilizing the ligand- $\alpha_{IIb}\beta_3$  receptor complex.

The external predictive  $R^2_{pred}$  was 0.72 for the CoMFA and 0.74 for the CoMSIA models, respectively (Table 2). Fig. 2C and D depict the correlations between the experimental and the predicted activities for both the training and test sets for the CoMFA and

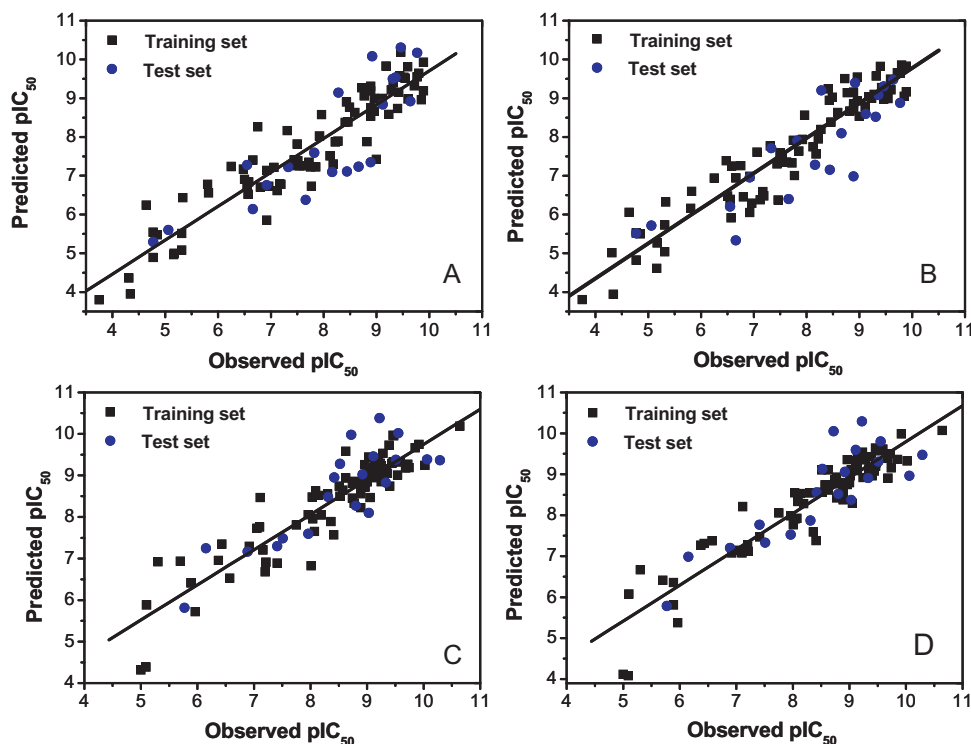


**Fig. 2.** The correlation plots of the predicted versus the actual  $pIC_{50}$  values using the training set (filled black square) and the test set (filled blue circle) based on the CoMFA and CoMSIA models obtained from activity for integrin  $\alpha_v\beta_3/\alpha_{IIb}\beta_3$ . The solid curves are the regression lines for the fitted and predicted bioactivities of the dataset. (A) CoMFA model for integrin  $\alpha_v\beta_3$ . (B) CoMSIA model for integrin  $\alpha_v\beta_3$ . (C) CoMFA model for integrin  $\alpha_{IIb}\beta_3$ . (D) CoMSIA model for integrin  $\alpha_{IIb}\beta_3$ . (For interpretation of the color information in this figure legend, the reader is referred to the web version of the article.)

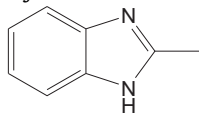
CoMSIA models respectively. Clearly, a good agreement between the predicted activities and experimental data was observed, and all the points are rather uniformly distributed around the regression line, suggesting the satisfactory predictive capability of the models.

### 3.3. Contour maps for integrin $\alpha_v\beta_3$

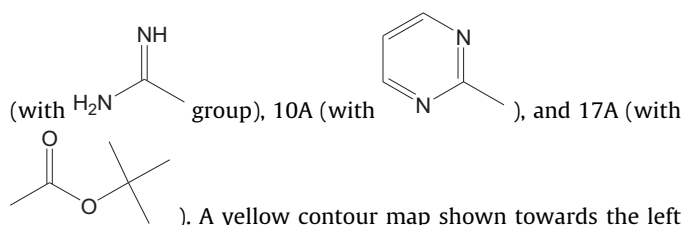
After consideration of both the internal and external predictive power of all the derived models, the best CoMFA and CoMSIA models are selected to construct the  $stdev \times coeff$  contour maps to view the field effects on the target features. The maps generated depict regions having scaled coefficients 80% (favored) or 20% (disfavored). To aid in visualization, the most active dual antagonist in the series (compound 10B) is shown superimposed with the CoMFA and CoMSIA contour maps (Fig. 3A and B and Fig. 4A–E). The coefficient contour plots are beneficial to identify important regions where some changes in the steric, electrostatic and hydrophobic fields may affect the biological activity, and in addition may also be of help to identify the possible interaction sites.

#### 3.3.1. CoMFA contour maps

For steric fields, Fig. 3A shows the sterically favored (green) and disfavored (yellow) regions of the molecule. The green contour mapped near the heterocyclic rings A and B, and benzene sulfonamide substituent of position 23, suggests that bulkier groups are favored at these positions. This discovery is well illustrated



by the example that compound 16A (with the substituent position) has higher activity than any other compound with smaller substituent at the same location like 15A



). A yellow contour map shown towards the left lower region of ring A indicates that the longer chain substituents towards this spatial distribution decrease the activity. The reason compound 31D shows less antagonist activity is just due to its substituents that is projected in the yellow region. Yellow blocks appeared at 23 position indicate that the bulky groups with longer chain substituents decrease the activity. This is confirmed by the loss of activity by compounds 38D and 39D which overlap on these blocks.

The electrostatic contour maps obtained from CoMFA analysis were mapped on to compound 10B as shown in Fig. 4B. The large size blue polyhedrons in the vicinity of position 23 and 24 indicate that the electropositive substituents at these regions such as C atom are disfavored. Compound 36A which have the lowest activity are showing that the ethyne on position 23 decreases the potency.

#### 3.3.2. CoMSIA contour maps

The CoMSIA steric and electrostatic contour maps (Fig. 4A and B) were similar to the ones obtained from the CoMFA model, and are thus not discussed here.

Fig. 4C shows the CoMSIA hydrophobicity field contour map, where the yellow (hydrophobic favorable) and white (hydrophobic unfavorable) contours represent 80% and 20% level contributions, respectively. Substitution by large hydrophilic groups like  $-NH_2$  at position 23 is extended to white region resulting in a higher integrin  $\alpha_v\beta_3$  antagonist activity, and when these hydrophilic groups such as  $-NH_2$ ,  $-OH$ ,  $-NHSO_2Ph$  were eliminated, the potency



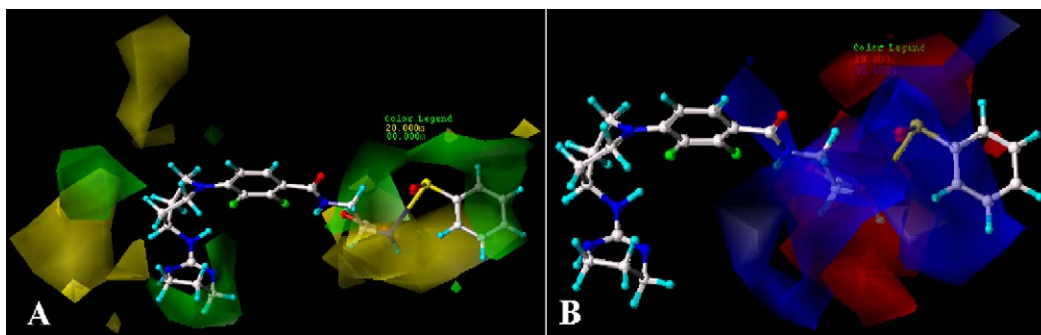


**Fig. 3.** CoMFA stdev\*coeff contour plots for integrin  $\alpha_v\beta_3$  in combination with compound 10B. (A) Steric (green/yellow) contour map. Green contours indicate regions where bulky groups increase activity; yellow contours indicate regions where bulky groups decrease activity. (B) Electrostatic contour map (blue/red). Blue contours indicate regions where negative charges increase activity; red contours indicate regions where positive charges increase activity. (For interpretation of the color information in this figure legend, the reader is referred to the web version of the article.)

fell off considerably, which can be exemplified by the higher activity of chemical 54B than 37B. Also a big yellow region is observed close to the white one indicating that ethyl group at the benzene ring D which is lyophobic radical can increase the activity.

Fig. 4D and E depict the H-bond donor and acceptor contour maps of the CoMSIA models. Cyan color indicates the regions where H-bond donor acts as favored and purple color refers to the disfavored regions. Magenta contours encompass regions where a H-bond acceptor will lead to improved biological activity, while

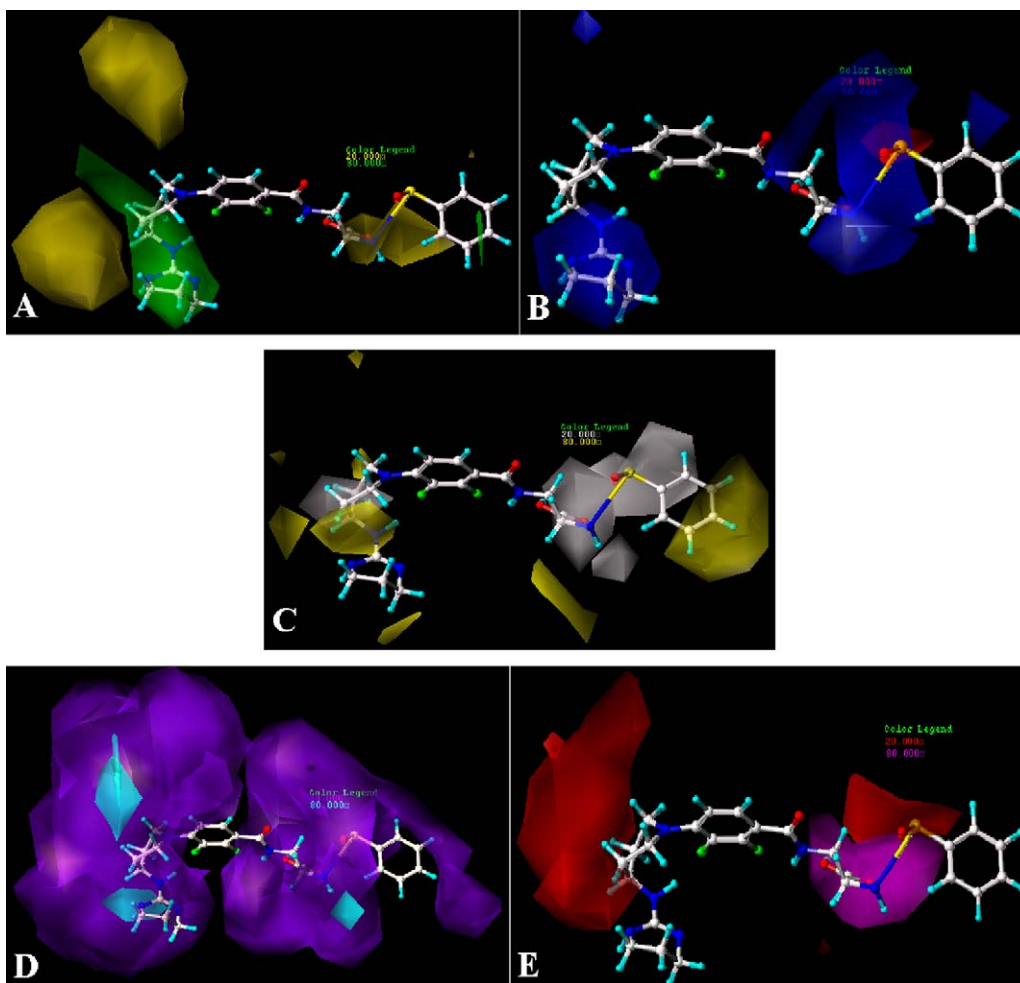


**Fig. 4.** CoMSIA stdev\*coeff contour plots for integrin  $\alpha_v\beta_3$  in combination with compound 10B. (A) Steric (green/yellow) contour map. Green contours indicate regions where bulky groups increase activity; yellow contours indicate regions where bulky groups decrease activity. (B) Electrostatic contour map (blue/red). Blue contours indicate regions where negative charges increase activity; red contours indicate regions where positive charges increase activity. (C) Hydrophobic contour map (yellow/white). Yellow contours indicate regions where hydrophobic substituents enhance activity; white contours indicate regions where hydrophobic substituents decrease activity. (D) CoMSIA contour maps illustrating hydrogen-bond donor features. The cyan contour represents the H-bond donor favored region, purple indicates the disfavored region. (E) CoMSIA contour maps illustrating hydrogen-bond acceptor features. The magenta contour indicates regions where H-bond acceptor groups increase activity, red contour indicates the disfavored region for H-bond acceptor groups. (For interpretation of the color information in this figure legend, the reader is referred to the web version of the article.)

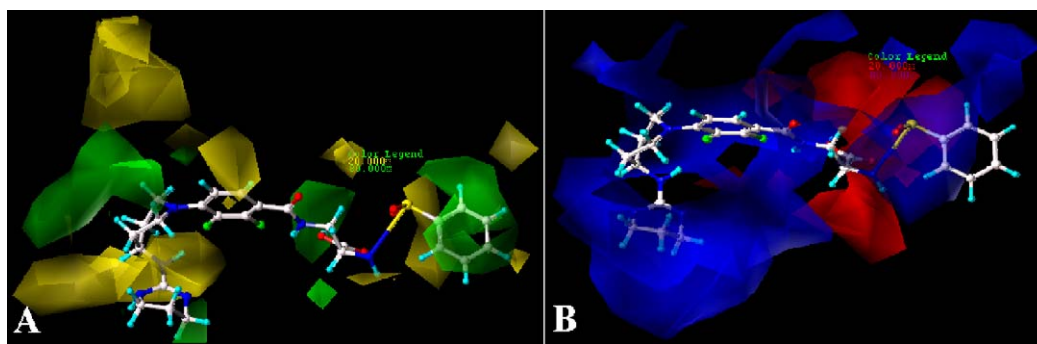


**Fig. 5.** CoMFA stdev\*coeff contour plots for integrin  $\alpha_{IIb}\beta_3$  in combination with compound 10B. (A) Steric (green/yellow) contour map. Green contours indicate regions where bulky groups increase activity; yellow contours indicate regions where bulky groups decrease activity. (B) Electrostatic contour map (red/blue). Red contours indicate regions where negative charges increase activity; blue contours indicate regions where positive charges increase activity. (For interpretation of the color information in this figure legend, the reader is referred to the web version of the article.)

an acceptor located near the red regions will result in impaired biological activity. In Fig. 4C, the purple contours around benzene ring C indicate that H-bond donor favors the activities but the presence of strong hydrogen bond acceptor is beneficial to the biological activity. Substitution by F and –OH groups at position 15, 16 of the benzene ring B is extended to show higher activities. The presence of strong H-bond acceptor in compound 10B is responsible for its high activity. Moreover, a big purple contour is observed surrounding position 23, suggesting that any H-bond donors are not favored in these areas. Compound 31A with –NH<sub>2</sub> at this position has lower activity than those have –NHSO<sub>2</sub>Ph instead. There is a magenta contour in Fig. 4E around position 23 indicating that H-bond acceptors are favored in these positions, which conclusion supports the above results depicted in Fig. 4C.

#### 3.4. Contour maps for integrin $\alpha_{IIb}\beta_3$

Like the  $\alpha_v\beta_3$  studies, the optimum CoMFA and CoMSIA models for  $\alpha_{IIb}\beta_3$  analysis are selected to construct the stdev\*coeff contour maps to view the field effects on the target features. The maps generated depict regions having scaled coefficients 80% (favored) or 20% (disfavored). To aid in visualization, compound 10B, as almost also the most active  $\alpha_{IIb}\beta_3$  antagonist in the series is shown superimposed with the CoMFA and CoMSIA contour maps (Figs. 5 and 6).

##### 3.4.1. CoMFA contour maps

For steric fields, Fig. 5A shows the contour maps of sterically favored (green) and disfavored (yellow) regions. Similar to the steric CoMFA contour maps for  $\alpha_v\beta_3$ , some green contours are mapped near the benzene ring D, suggesting that bulkier groups are favored at these positions. The fact that compound 44B (having –SO<sub>2</sub>C<sub>6</sub>H<sub>2</sub>-2,4,6-Tri-Me at the areas) is more potent in activity than 22B (having –SO<sub>2</sub>Ph) is a good example. Another yellow contour map was also observed appearing at the left lower region of benzene ring B indicating that the bulkier chain substituents at position 12 towards this spatial distribution decrease the activity. Compound 33D which shows less activity with –OCH<sub>3</sub> substituent at position 12 proves this conclusion.

Fig. 5B shows the electrostatic contour maps obtained from the CoMFA analysis with compound 10B shown as the template. The large blue polyhedron surrounding almost the whole molecule indicates its favor for the electropositive charged substituents. The fact that compounds 8B, 9B, 10B, 11B, and 12B of high activity all possess strong electronegative atoms including the halogen and oxygen atoms on the position C15 or C16 of the ring C proves this

finding. Molecule 33C which has N=C(N)N (instead of ring A at the position) shows higher activity than those molecules with ring A including 10C, 27C, 28C and 31C is another good illustration. The presence of red contour map at the N atom of benzene sulfonamide substituent indicates that electronegative groups attached at this position show improved activity, as observed in the compound 1B against the unsubstituted compound 37B.

##### 3.4.2. CoMSIA contour maps

Since similar results are obtained for the steric and electrostatic contours of CoMSIA as those of the CoMFA model (Fig. 5), only the characteristics of the hydrophobic and hydrogen bonding interaction fields are described here.

For the CoMSIA hydrophobicity field contour map (Fig. 6C), the yellow (hydrophobic favorable) and white (hydrophobic unfavorable) contours represent 80% and 20% level contributions, respectively. The appearance of white contours at position 15, 16 and 23 indicates that substitution by hydrophilic groups at these locations is extended to result in a higher integrin  $\alpha_{IIb}\beta_3$  antagonist activity. For example, compound 9B with –Cl at position 15 and –NHSO<sub>2</sub>Ph at position 23 has the highest activity in the dataset. Close to the benzene ring D a big yellow contour is also observed suggesting that ethyl group which is hydrophobic radical at this area such as 42D can increase the activity.

Fig. 6D and E depict the H-bond donor and acceptor contour maps of the CoMSIA models. In Fig. 6D, the H-bond donor plot, the cyan contours indicate regions where hydrogen bond donor substituents on the ligands are favored and purple contours represent areas where hydrogen bond donor properties on antagonists are disfavored. Some green contour maps surrounding the heterocyclic ring B are observed, illuminating the areas' favor for H-bond donor substituents. The presence of strong H-bond donor in compound 36D is responsible for its higher activity than 37D. Around benzene ring C a cyan contour shows up indicating where H-bond donors decrease the activity. For example, the antagonistic activity of compound 12B is lower than 9B is just due to the –OH instead of –Cl group at position 15. In Fig. 6E, the H-bond acceptor map, the magenta contours represent regions where hydrogen bond acceptors on the ligands are favorable and red contours indicate regions where hydrogen bond acceptors are unfavorable for the activity. In Fig. 6E, the red contours over position 23 and 24 indicate that presence of strong H-bond acceptor is detrimental to the biological activity. Substitution by –OH groups at position 23 of 36B is extended to showed higher activity than 39B.

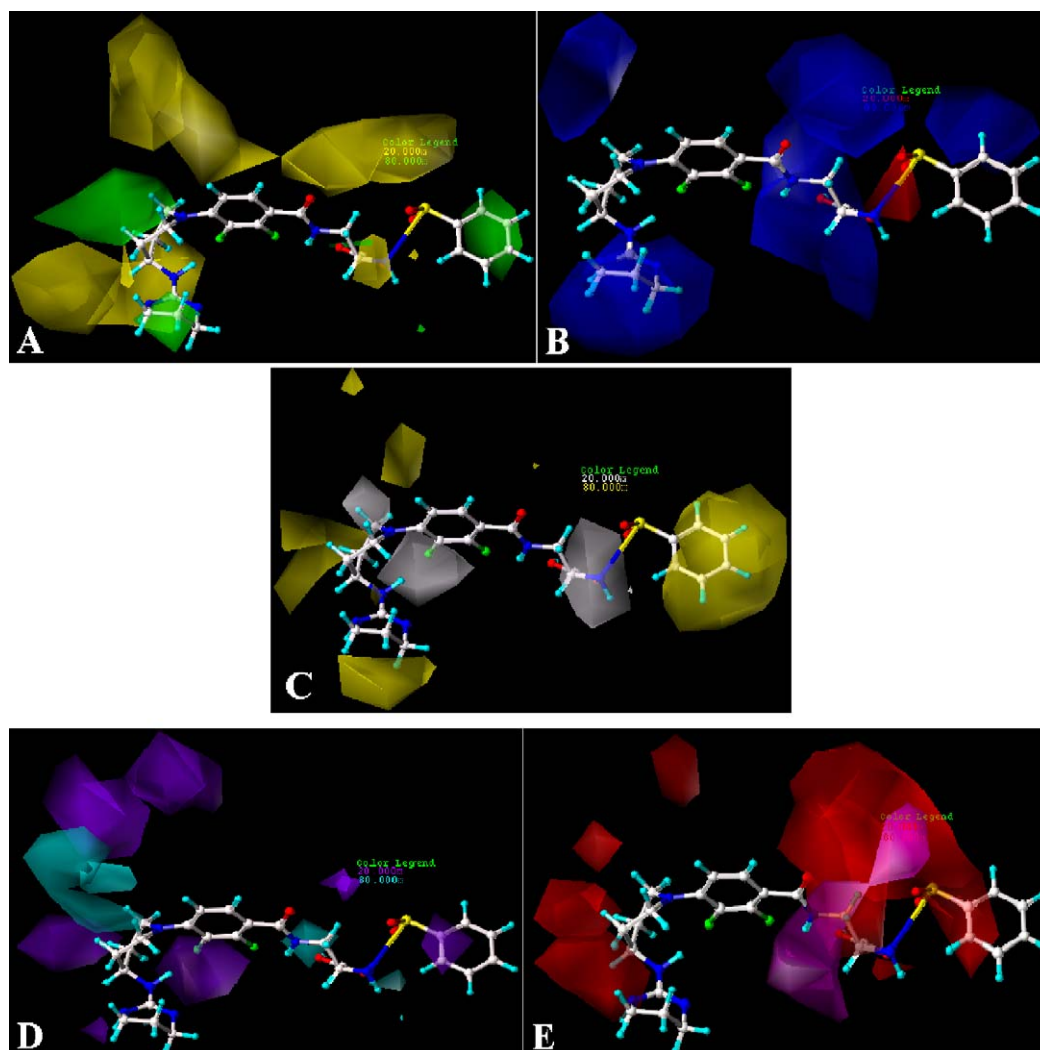


**Fig. 6.** CoMSIA stdev\*coeff contour plots for integrin  $\alpha_{IIb}\beta_3$  in combination with compound 10B. (A) Steric (green/yellow) contour map. Green contours indicate regions where bulky groups increase activity; yellow contours indicate regions where bulky groups decrease activity. (B) Electrostatic contour map (blue/red). Blue contours indicate regions where negative charges increase activity; red contours indicate regions where positive charges increase activity. (C) Hydrophobic contour map (yellow/white). Yellow contours indicate regions where hydrophobic substituents enhance activity; white contours indicate regions where hydrophobic substituents decrease activity. (D) CoMSIA contour maps illustrating hydrogen-bond donor features. The cyan contour represents the H-bond donor favored region, purple indicates the disfavored region. (E) CoMSIA contour maps illustrating hydrogen-bond acceptor features. The magenta contour indicates regions where H-bond acceptor groups increase activity, red contour indicates the disfavored region for H-bond acceptor groups. (For interpretation of the color information in this figure legend, the reader is referred to the web version of the article.)

### 3.5. Docking studies

In order to find the optimal orientation of the ligand in the binding pocket of the protein, docking studies were also carried out on the dataset [41]. In our work, all 102 compounds in the dataset were docked into the possible active site of integrin  $\alpha_v\beta_3$  and  $\alpha_{IIb}\beta_3$  crystal structures, and the optimal conformations of these compounds were determined. Our results show that all the molecules in the series were placed well in the active site demonstrating the quality of the docking model. The binding mode of the highly potent compound 10B docked into the receptors is taken as an example.

#### 3.5.1. For integrin $\alpha_v\beta_3$

Compound 10B was used as a template to show the docking modes of integrin  $\alpha_v\beta_3$  (PDB entry: 3IJE) and  $\alpha_{IIb}\beta_3$  (PDB entry: 2VDM) inhibitors, since this compound exhibited the most potent antagonistic activity against both of them. Stereo diagram showing the interactions of integrin  $\alpha_v\beta_3$  with antagonist 10B is provided in Fig. 7, where the hydrogen bonds between the antagonist and

the protein molecule are shown as dashed lines. In Fig. 7A, yellow oval plate is for  $\alpha$  subunit, and blue oval plate is for  $\beta$  subunit, respectively.

The N atom of the heterocyclic ring A accepts a H-bond ( $-N \cdots H-N-$ ) (2.72 Å) from Arg214 of  $\beta$  chain in the crossover connection. And the  $-N-H-$  group at this position provides another H-bond ( $-N-H \cdots H-$ ) (1.99 Å) to Asn215 of  $\beta$  chain. Moreover, the  $-N-H-$  group of Arg214 provides another H-bond (3.03 Å) to the N atom of position 7. The H-bonds interactions at the ring A may favor the activity which was shown by the cyan and red contours of the left domain at the H-bond contour maps (Fig. 4D and E). From the H-bond donor and acceptor contour maps for CoMSIA models, it is known that H-bond acceptor interactions can increase the antagonistic activity. Correspondingly, two H-bonds ( $-O \cdots H-N-$ ) (2.69 Å and 1.89 Å) are also observed in the binding pocket at the substituents of position 23 and 24 to Lys253 of  $\beta$  chain, respectively. However, the F atom at position 16 also accepts a H-bond ( $-F \cdots H-O-$ ) (2.67 Å) to Ser123 of  $\beta$  chain. In a word, once again H-bond is found crucial for the interaction between the new fused antagonists and integrin  $\alpha_v\beta_3$  receptor.



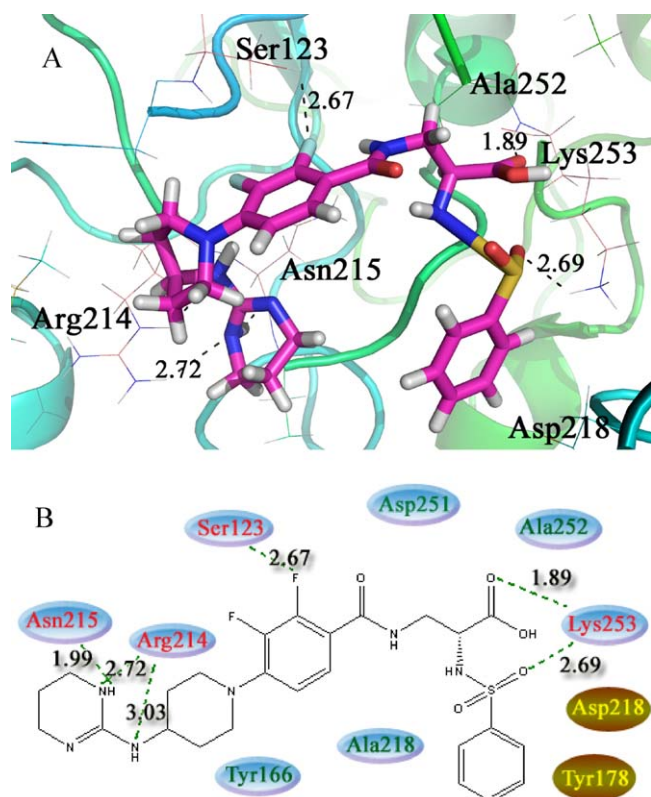


**Fig. 7.** Molecular models of Compound 10B in the binding site of integrin  $\alpha_v\beta_3$  (3IJE). (A) Representative interactions with amino acids of  $\alpha_v\beta_3$ . The dashed lines show the formation and distance of the hydrogen bonds. Active site amino acid residues are represented as lines, the antagonist is shown as stick model. (B) 2D representation of the antagonist 10B and integrin binding domain of  $\alpha_v\beta_3$ . Yellow oval plate is for  $\alpha$  subunit, and blue oval plate is for  $\beta$  subunit, respectively. Amino acids in red are the residuals having hydrogen interactions with antagonist 10B, in other colors are those close to 10B which may impact the ligand- $\alpha_v\beta_3$  interactions in the binding pocket. (For interpretation of the color information in this figure legend, the reader is referred to the web version of the article.)

Our docked model also shows a comparatively large empty space around the heterocyclic ring A and benzene ring D, indicating that in these regions the steric interaction may be favorable. The conclusions are similar to the above CoMFA and CoMSIA contour maps analysis (Figs. 4A and 5A). In addition, some hydrophilic amino acids are found around the specific positions in the molecule, including residues Lys253 and Asp219 (data not shown in the figure) surrounding the sulfonamide group, and Arg214 and Asn215 near ring B, indicating that hydrophilic substituents at position 23 and heterocyclic ring A are beneficial to enhance the activity. This conclusion is consistent with previous contour map results.

Recently, M. Ishikawa et al. also carried out a docking study by docking compounds 1C, 10C, 21C into  $\alpha_v\beta_3$  receptor [24]. Although the docking pocket is the same one as used in our study, their conclusions are somewhat different from ours. Similar to us, Arg214 is also found as crucial hydrogen bonding interaction residue. But the other hydrogen binding residues or important binding groups of the compounds they identified are different. They found that the major interactions were hydrogen bonding of NH at N-terminus with Tyr122 and Arg214 in the  $\beta$  chain and Asp218 in the  $\alpha$  chain, coordination of the carboxyl group at C-terminus. But in our work, the hydrogen bonding residues are Arg214 which is the same one, and Asn215, Ser123 and Lys253.

The reasons for the difference may be as follows. Firstly, the PDB entry differs that 1L5G was used as the docked structure of  $\alpha_v\beta_3$  receptor in M. Ishikawa's work while 3IJE was chosen in our work. Moreover, their results were built only by docking three antagonists

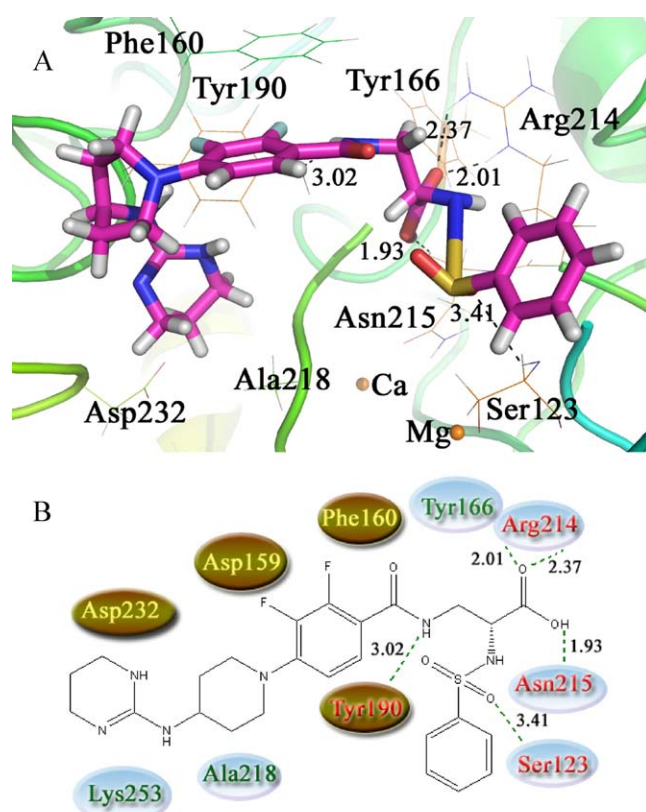


**Fig. 8.** Molecular models of Compound 10B in the binding site of integrin  $\alpha_{11b}\beta_3$  (2VDM). (A) Representative interactions with amino acids of  $\alpha_{11b}\beta_3$ . The dashed lines show the formation and distance of the hydrogen bonds. Active site amino acid residues are represented as lines, the antagonist is shown as stick model. (B) 2D representation of the antagonist 10B and integrin binding domain of  $\alpha_{11b}\beta_3$ . Yellow oval plate is for  $\alpha$  subunit, and blue oval plate is for  $\beta$  subunit, respectively. Amino acids in red are the residuals having hydrogen interactions with antagonist 10B, in other colors are those close to 10B which may impact the ligand- $\alpha_{11b}\beta_3$  interactions in the binding pocket.

into the receptor, but ours is obtained by docking and analyzing all of the 102 molecules into integrin  $\alpha_v\beta_3$ , which may promote the generalization and application of our models. Thirdly, the range of the activity is different, with  $pIC_{50}$  values from 6.495 to 9.319 for their study while from 3.745 to 9.886 for ours.

### 3.5.2. For integrin $\alpha_{11b}\beta_3$

The binding mode of compound 10B docked into human integrin  $\alpha_{11b}\beta_3$  (PDB entry: 2VDM) is shown in Fig. 8. It is found that the backbone -NH- in Arg214 may form two H-bonds with the -C=O group at position 24 in 10B, the distance of which is 2.01 Å and 2.37 Å, respectively. Between the backbone -O- in the Asn215 and the -OH- group at position 24 forms a H-bond, with a distance of 1.93 Å. Also between the backbone -O- in the Tyr190 and the -NH- group at position 20 of 10B forms a H-bond of distance of 3.02 Å. Moreover, there may have a H-bond (-O...HN- 3.41 Å) at the substituent benzene sulfonamide to Ser123 of  $\beta$  chain. All these results are well consistent with above CoMSIA contour maps.

Fig. 8B shows the 2D representation binding patterns for compound 10B, where the yellow oval plate is for  $\alpha$  subunit, and blue oval plate is for  $\beta$  subunit, respectively. From the analysis of our CoMSIA contour maps, similar conclusions are made. As seen from Fig. 6E, obviously the H-bonds may form at the regions around position 20 to 24 and sulfonamide substituent between the integrin  $\alpha_{11b}\beta_3$  receptor and molecules. The hydrogen binding interactions in the binding pocket also show that H-bonds are very important for

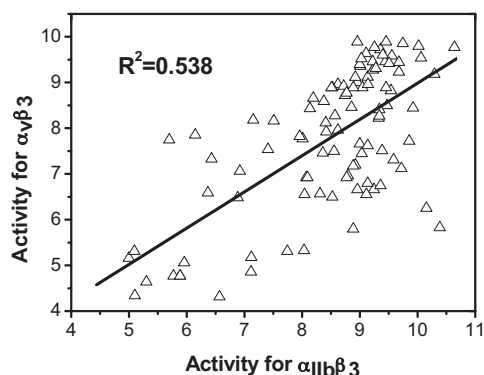


Fig. 9. A correlation plot of activities for  $\alpha_v\beta_3$  and  $\alpha_{IIb}\beta_3$  of all dataset.

the interaction between these new fused antagonists and integrin  $\alpha_{IIb}\beta_3$  receptor.

Our docked model also shows that near the heterocyclic ring D position the amino acid residues are absent, indicating where a favorable steric interaction may be favorable, and this conclusion is similar to the above CoMFA and CoMSIA contour map analysis (Figs. 5A and 6A). In addition, hydrophilic amino acids Arg214, Asn215 appear around sulfonamide substituent, which is similar to the hydrophobic contour maps in Fig. 6C with white region at position 23 of 10B.

### 3.6. Comparison for integrin $\alpha_v\beta_3$ and $\alpha_{IIb}\beta_3$

#### 3.6.1. Comparison of two antagonistic activities

To investigate the possible relationship between the two antagonist activities for integrin  $\alpha_v\beta_3$  and  $\alpha_{IIb}\beta_3$ , a mathematical model was established between the two activities based on all compounds except two chemicals with unavailable activity data defined, and the result reveals that the activities of the 100 tricyclic piperazine/piperidine furnished molecules to inhibit the integrin  $\alpha_v\beta_3$  and  $\alpha_{IIb}\beta_3$  were obviously linear correlated with a correlation coefficient of  $R^2 = 0.538$ . Fig. 9 shows the correlation between them, which illustrates that activity for  $\alpha_v\beta_3$  is in good agreement with that for  $\alpha_{IIb}\beta_3$ , suggesting that in general those  $\alpha_v\beta_3$  antagonists can also effectively inhibit  $\alpha_{IIb}\beta_3$  (which is consistent with the results reported previously).

As reported, the research into  $\alpha_v\beta_3$  has benefited great from the discoveries made in the  $\alpha_{IIb}\beta_3$  research whose area is more mature. Upon activation of  $\alpha_{IIb}\beta_3$  and subsequent fibrinogen binding, platelets are cross-linked resulting in the platelet aggregation [8]. If the activation status of the integrin  $\alpha_{IIb}\beta_3$  was improperly regulated platelet aggregation and subsequently thrombosis would ultimately occur. However, though the interaction between  $\alpha_v\beta_3$  and the platelet aggregation is not fully defined as the  $\alpha_{IIb}\beta_3$ , it can either lead to migration or adhesion of the cell to a particular substrate [42]. As known that blocking fibrinogen binding to  $\alpha_{IIb}\beta_3$  can finally inhibit the final step of platelet aggregation [43], the  $\alpha_v\beta_3$  may have same functional in platelet aggregation.

#### 3.6.2. Structural superposition of proteins

The crystal structure superposition of integrin  $\alpha_v\beta_3$  (PDB 3IJE) and  $\alpha_{IIb}\beta_3$  (PDB 2VDM) were created using <http://cl.sdsc.edu/> [44], and the comparison of similarities of the two proteins is summarized in Table 3. For PDB 2VDM, H and L chains were included for that hemostasis and thrombosis (blood clotting) involve fibrinogen binding to integrin  $\alpha_{IIb}\beta_3$  on platelets, resulting in the platelet aggregation [37]. PDB 3IJE (USR1) and 2VDM (USR2) both contained two similar chains, i.e.,  $\alpha$  and  $\beta$  chains (A and B chains in Fig. 10, respectively).

Table 3

Comparison of the crystal structures of integrin  $\alpha_v\beta_3$  (3IJE) and  $\alpha_{IIb}\beta_3$  (2VDM).

Comparative chains	3IJE:A-2VDM:A	3IJE:B-2VDM:B
Rmsd (Å)	1.5	2.6
Z-score	7.8	7.2
Sequence identity	44.50%	89.10%
Aligned/gap positions	422/47	248/6

Comparison of integrin  $\alpha_v\beta_3$  and  $\alpha_{IIb}\beta_3$ , the two integrin heterodimeric receptors, shows that they consist of two subunits including a common  $\beta_3$  subunit. And these integrins have inter-domain structure consistent with the parallel-sandwich-hybrid topology of the subunit domain integrins [45].

As shown in Table 3, the aligned Rmsd were 1.5 Å and 2.6 Å, with the Z-score of 7.8 and 7.2, for the two comparative chains respectively. Moreover, the sequence identity was 89.10% for the  $\beta$  chain, which indicate that the  $\beta$  chain has more similarity as a common subunit. Fig. 10 shows the alignments of the sequences of 3IJE and 2VDM for chains A and B. The binding sites of antagonist 10B are highlighted in black rectangles. In the figure it can be seen that the sequence ID of the  $\beta$  chain (USR B) for  $\alpha_v\beta_3$  from 105 to 334 is almost the same as  $\alpha_{IIb}\beta_3$ . Therefore, we can conjecture that the docking domain for  $\alpha_v\beta_3$  and  $\alpha_{IIb}\beta_3$  may have the same active sites.

The structural superposition of the 3IJE to 2VDM is shown in Fig. 11, indicating that the overall conformation of the modeling target is very similar to the template. And almost all key amino acids of  $\beta$  subunit (such as Ser121, Tyr122, Ser123, Tyr166, Met180, Arg214, Arg216, Asp217, Ala218, Asp251, Ala252 and Lys253) interacting with the tricyclic pharmacophore-based molecules in the binding site are well overlaid in 3D space in the two structures. Therefore, though the binding site for  $\alpha_v\beta_3$  is not clearly reported, it can be assumed that it is the same as the site of  $\alpha_{IIb}\beta_3$  which has been reported.

#### 3.6.3. Comparison of the 3D-QSAR results

In general, the comparison of the CoMFA and CoMSIA statistical results for integrin  $\alpha_v\beta_3$  and  $\alpha_{IIb}\beta_3$  studies (Table 2) reveals that, excepting for subtle difference, very similar results were obtained for the two receptors. Firstly, both the optimal 3D-QSAR models were built by using same descriptor group, i.e., the CoMFA models for  $\alpha_v\beta_3$  and  $\alpha_{IIb}\beta_3$  both used the steric and electrostatic fields, while the CoMSIA ones for  $\alpha_v\beta_3$  and  $\alpha_{IIb}\beta_3$  both employed all five interaction fields. This indicates that for the binding of ligands to both  $\alpha_v\beta_3$  and  $\alpha_{IIb}\beta_3$ , the interaction fields impacting this binding may be the same. Secondly, both the steric and electrostatic fields are found crucial to the receptor-ligand interactions, where the former contributes about 60% and the latter approximately 40% to the activities demonstrated by the CoMFA results. Besides, hydrogen-bonds are demonstrated again playing crucial roles for the interactions, with a sum of contributions of 53% (H-bond donor: 36%, H-bond acceptor: 17%) and 47% (H-bond donor: 29%, H-bond acceptor: 18%) in the CoMSIA models for  $\alpha_v\beta_3$  and  $\alpha_{IIb}\beta_3$ , respectively.

#### 3.6.4. Comparison of the 3D-QSAR contour maps

Analysis of the 3D-QSAR contour maps derived from activity for integrin  $\alpha_v\beta_3$  and  $\alpha_{IIb}\beta_3$  (Figs. 3–6) suggests that they have very similar structural requirements for potent ligands. As discussed above, the steric contour maps illustrate that bulky groups such as benzimidazole could possibly increase the antagonistic activity near position 3 of the imidazole ring A. Furthermore, hydrophobic residues at the benzene ring C would result in an increase of the activity, but a small polar hydrophilic residue near the benzene ring B might be favorable as illustrated by the white contours in



USR1:A	1/2	FNLDVDSPAEYSGFEGSYFGFAVDFVFPASASSRMLLVGAPKANTTQPGIVEGGQVLKCD
USR2:A	1/2	LNLDPVQLTTFVAGNGSQFGSLDFHKD-SHGEVAIVVGAPRTLGP--SQETGGVFLCP
USR1:A	61/62	WSS-TRRCQPIEFDATGNRD-----YAKDDPLEFKSHQWFGASVRSKQDKILACAPLY
USR2:A	58/59	WRAEGGQCPSSLFD-LRDETRNVGSQTL-----QTFKARQGLGASVVSIVIVACAPWQ
USR1:A	113/114	HURTEM---KQEREPUVGTCTFLQDG--TKTVEYAPCRSQ-----DIDADGGQFC
USR2:A	112/113	HUNVLEKTEEAETPVGSCFLAQPESSGRRAEYSPCRGNTLSRIYVENIFSW---DKRYC
USR1:A	156/157	QGGSIDFTKADRVLLGGPGSFYWGQQLISDQVAETVSHYDPNVYSIKYNNQLATRTAQA
USR2:A	168/169	EAGFSSVVTQAGELVLGAPGGYFLGLLAQAPVADIFSSYRPGILLWHVSSQSLSDSSN
USR1:A	216/217	I-FIDSYLGYSVAUGDFNGDG-IDDFVSGVPRAARTLGMWYIYDGKNNSSLYNFTGEQMA
USR2:A	228/229	PEYFEGYUGYSVAUGDFDGLNLTTEYVVGAPTWSTLGAVEILDS-YYQLRHRLRGEQMA
USR1:A	274/275	AYFGFSAATDINGDDYADVFIGAPLFMDRGSDGKLQEVGVSVSLQAS-GDFQ--TTK
USR2:A	287/288	SYFGHSAVTDVNGDGRHDLVVGAPLYMESRADRKLAEGVRVYFLQPRGPHALGAPSL
USR1:A	331/332	LNGFEVFARFGSAIAPLGDLDDQDFNDIAIAAPYGGEDKKGIYIFNGRSTGLNAVPSQI
USR2:A	347/348	LTGTQLYGRFGSAIAPLGDLDRDGYNDIAVAAPYGGPSGRGQVLVFLGQSGELSRPSQV
USR1:A	391/392	LEGQWAARSMPSPFGYSMKGATDIDKNGYPDLIVGAFGVDRAILYRARP
USR2:A	407/408	LDSPFPT---GSAFGFSLRGAVDIDNGYPDLIVGATGANQVAVYRAQP
USR1:B	105/106	RQVEDYPVDIYYLMDLSYSMKDDLWSIQNLGTLKATQMRKLTSLNLRIGFGAFVDKPVSPY
USR2:B	105/106	RQVEDYPVDIYYLMDLSYSMKDDLWSIQNLGTLKATQMRKLTSLNLRIGFGAFVDKPVSP-
USR1:B	165/166	MYISPPEALE-NPCYDMKTTCLHFGYKHVLTLDQVTRFNEEVKKQSVSRNRDAPEGGF
USR2:B	164/165	YMYISPPEALENPCYDMKTTCLHFGYKHVLTLDQVTRFNEEVKKQSVSRNRDAPEGGF
USR1:B	224/225	DAIMQATVCDEKIGWRNDASHLLVFTTDAKTHIALDGRLAGIVQPNQGCHVGSNDHYS
USR2:B	224/225	DAIMQATVCDEKIGWRNDASHLLVFTTDAKTHIALDGRLAGIVQPNQGCHVGSNDHYS
USR1:B	284/285	STTMDYPSLGLMTEKLSQKNINLIFAVTENVVNLYQNYSELIPGTTVGVLSDMSNNVLQ
USR2:B	284/285	STTMDYPSLGLMTEKLSQKNINLIFAVTENVVNLYQNYSELIPGTTVGVLSDMSNNVLQ
USR1:B	344/345	IVDAYGKIRSKVEL
USR2:B	340/341	VLQLIVDAYGKIRS

**Fig. 10.** Alignments of the sequences of 3IJE and 2VDM for chains A and B. USR1 is for 3IJE, and USR2 is for 2VDM. Light green color regions denote that the amino acid residues in the individual column are identical in the sequence alignment. Dashed lines denote the amino acid residues deletion. The binding sites of antagonist 10B are highlighted in black rectangles. (For interpretation of the color information in this figure legend, the reader is referred to the web version of the article.)

Figs. 4 and 6. However, it can be seen from the purple contours maps in the Fig. 4D and E, that any H-bond donors surrounding the benzene ring B position are not favored in these areas. The red contours showed at the same areas in both Figs. 4E and 6E indicate that the presence of strong H-bond acceptor is detrimental to the biological activity.

Although the similarities between the contour maps of two activities help us finding the potent active molecule, the differences between them also make good assistance. Firstly, in CoMFA models no blue regions are found around rings A and B for activity of  $\alpha_v\beta_3$  but a big blue contour exists for  $\alpha_{IIB}\beta_3$  indicating that negative charged groups enhance the antagonistic activity to  $\alpha_{IIB}\beta_3$  but may have no impact on  $\alpha_v\beta_3$  antagonist potency. Next, H-bond interaction may contribute larger to enhance the activity for  $\alpha_v\beta_3$  over  $\alpha_{IIB}\beta_3$  as there are bigger purple regions in CoMSIA contour maps for  $\alpha_v\beta_3$ .

The reasons for above similarities and differences may be as follows. Integrin  $\alpha_v\beta_3$  and  $\alpha_{IIB}\beta_3$  are almost the same in their  $\beta$  subunit, with many common amino acid sequences, which may result in the very similar structural features of the antagonists. However, comparatively large difference still exists in their  $\alpha$  subunit, which substructure may finally determine their specific requirements for their “favorite” ligands.

### 3.6.5. Selectivities for $\alpha_v\beta_3$ over $\alpha_{IIB}\beta_3$

According to the 3D-QSAR and docking analyses, several interesting phenomena were discovered. Firstly, the place and size of substituent at central benzene ring C was found may, to some extents, influence the selectivity for  $\alpha_v\beta_3$  over  $\alpha_{IIB}\beta_3$ . Clearly, by meta-oriented substitution other than para-substituent of the central benzene ring, the selectivity of the molecules is enlarged which is indicated by the result that molecule 22D shows higher selec-

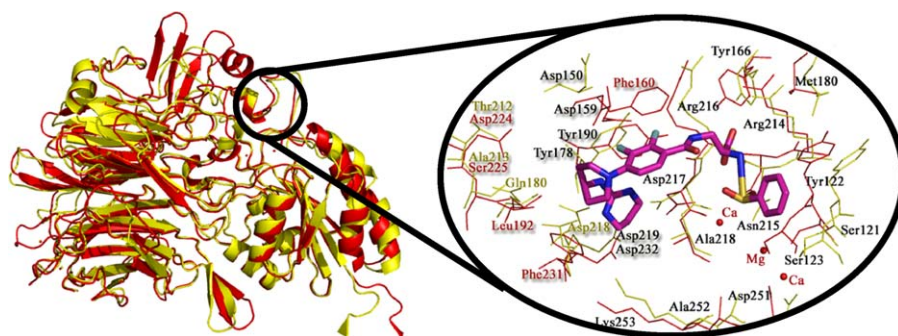


**Fig. 11.** Structural superposition of  $\alpha_v\beta_3$  (3IJE) and  $\alpha_{IIB}\beta_3$  (2VDM). The projection highlights the structure of the active site with antagonist 10B which is displayed in sticks. The same residues are labeled in black color, while the different residues between them are labeled in their own color.

tivity than 1B. Secondly, when big substituent at position 15 of central benzene ring C was selected, the selectivity for  $\alpha_v\beta_3$  over  $\alpha_{IIb}\beta_3$  was also improved. For example, 47D with  $-\text{CF}_3$  at position 15 exhibited marked selectivity for  $\alpha_v\beta_3$  over  $\alpha_{IIb}\beta_3$ . In addition, shorter and hydrophilic substituent of ring B like piperazine may disfavor the selectivity for  $\alpha_v\beta_3$  over  $\alpha_{IIb}\beta_3$ . This is well demonstrated by compounds 4A, 10A, 15A and 17A. Though differ subtly at ring A, they all have a same substituent of piperazine at ring B, and thus all showing weak antagonistic activities to  $\alpha_v\beta_3$  but strong  $\alpha_{IIb}\beta_3$ -antagonistic activities (with selectivity all below 0.01).

#### 4. Conclusion

In this paper, the ligand-based and receptor-based 3D-QSAR studies of 102 tricyclic piperazine or piperidine furnished dual antagonists of  $\alpha_v\beta_3$  and  $\alpha_{IIb}\beta_3$  were, for the first time, performed using CoMFA and CoMSIA tools. The constructed 3D-QSAR models exhibited proper predictive powers in both the internal and external tests. The resulting contour maps produced by the models provide useful information about the intermolecular interactions of the antagonists with the surrounding environment. A good consistency between the CoMFA and CoMSIA contour maps and the docking results was observed, proving the reliability and robustness of the models. Overall, our main findings are summarized as follows:

- (1) H-bond properties of the molecules play important roles for their antagonistic activity against both the  $\alpha_v\beta_3$  and  $\alpha_{IIb}\beta_3$ , that most H-bond donor and/or acceptor substituents like  $-\text{NH}-$ ,  $-\text{F}$ ,  $-\text{COOH}$  might be favorable for the ligand binding.
- (2) Halogen-containing groups at position 15 and 16, benzene sulfonamide substituent at position 23, and the replacement of piperazine with 4-aminopiperidine of ring B may increase the  $\alpha_v\beta_3/\alpha_{IIb}\beta_3$  antagonistic activity.
- (3) The potencies for antagonists to inhibit isolated  $\alpha_v\beta_3$  and  $\alpha_{IIb}\beta_3$  are linear correlated (with a coefficient  $R^2 = 0.538$ ), indicating that similar interaction mechanisms may exist for the series of molecules.
- (4) Key amino acids impacting the receptor-ligand interactions are Arg214, Asn215, Ser123, and Lys253 for  $\alpha_v\beta_3$ , but Arg214, Asn215, Ser123 and Tyr190 for  $\alpha_{IIb}\beta_3$  receptors, respectively.

#### Acknowledgment

We thank Dr. Ming Hao for helpful discussion. And this work is financially supported by the National Natural Science Foundation of China (Grants No. 10801025).

#### Appendix A. Supplementary data

Supplementary data associated with this article can be found, in the online version, at doi:10.1016/j.jmgm.2010.12.008.

#### References

- [1] W.H. Frishman, B. Burns, B. Atac, N. Alturk, B. Altajar, K. Lerrick, Novel antiplatelet therapies for treatment of patients with ischemic heart disease: Inhibitors of the platelet glycoprotein IIb/IIIa integrin receptor, *Am. Heart. J.* 130 (1995) 877–892.
- [2] D. Kubota, M. Ishikawa, M. Yamamoto, S. Murakami, M. Hachisu, K. Katano, K. Ajito, Tricyclic pharmacophore-based molecules as novel integrin  $\alpha_v\beta_3$  antagonists. Part I: Design and synthesis of a lead compound exhibiting  $\alpha_v\beta_3/\alpha_{IIb}\beta_3$  dual antagonistic activity, *Bioorg. Med. Chem.* 14 (2006) 2089–2108.
- [3] L. Marinelli, A. Lavecchia, K.-E. Gottschalk, E. Novellino, H. Kessler, Docking studies on  $\alpha_v\beta_3$  integrin ligands: pharmacophore refinement and implications for drug design, *J. Med. Chem.* 46 (2003) 4393–4404.
- [4] A.P. Silverman, A.M. Levin, J.L. Lahti, J.R. Cochran, Engineered cystine-knot peptides that bind  $\alpha_v\beta_3$  integrin with antibody-like affinities, *J. Mol. Biol.* 385 (2009) 1064–1075.
- [5] D. Elliot, E. Henshaw, P.A. MacFaul, A.D. Morley, P. Newham, K. Oldham, K. Page, N. Rankine, P. Sharpe, A. Ting, C.M. Wood, Novel inhibitors of the  $\alpha_v\beta_3$  integrin: lead identification strategy, *Bioorg. Med. Chem. Lett.* 19 (2009) 4832–4835.
- [6] D.G. Metcalf, D.W. Kulp, J.S. Bennett, W.F. DeGrado, Multiple approaches converge on the structure of the integrin  $\alpha_{IIb}\beta_3$  transmembrane heterodimer, *J. Mol. Biol.* 392 (2009) 1087–1101.
- [7] K.M. Hodivala-Dilke, K.P. McHugh, D.A. Tsakiris, H. Rayburn, D. Crowley, M. Ullman-Culleré, F.P. Ross, B.S. Coller, S. Teitelbaum, R.O. Hynes,  $\beta_3$ -integrin-deficient mice are a model for glanzmann thrombasthenia showing placental defects and reduced survival, *J. Clin. Invest.* 103 (1999) 229–238.
- [8] I.G. Ahrens, N. Moran, K. Aylward, G. Meade, M. Moser, D. Assefa, D.J. Fitzgerald, C. Bode, K. Peter, Evidence for a differential functional regulation of the two  $\beta_3$ -integrins  $\alpha_v\beta_3$  and  $\alpha_{IIb}\beta_3$ , *Exp. Cell Res.* 312 (2006) 925–937.
- [9] J.S. Bennett, C. Chan, G. Vilaine, S.A. Mousa, W.F. DeGrado, Agonist-activated  $\alpha_v\beta_3$  on platelets and lymphocytes binds to the matrix protein osteopontin, *J. Biol. Chem.* 272 (1997) 8137–8140.
- [10] M. Ishikawa, D. Kubota, M. Yamamoto, C. Kuroda, M. Iguchi, A. Koyanagi, S. Murakami, K. Ajito, Tricyclic pharmacophore-based molecules as novel integrin  $\alpha_v\beta_3$  antagonists. Part 2: Synthesis of potent  $\alpha_v\beta_3/\alpha_{IIb}\beta_3$  dual antagonists, *Bioorg. Med. Chem.* 14 (2006) 2109–2130.
- [11] W.J. Pitts, J. Wityak, J.M. Smallheer, A.E. Tobin, J.W. Jetter, J.S. Buynitsky, P.P. Harlow, K.A. Solomon, M.H. Corjay, S.A. Mousa, R.R. Wexler, P.K. Jadhav, Isoxazolines as potent antagonists of the integrin  $\alpha_v\beta_3$ , *J. Med. Chem.* 43 (1999) 27–40.
- [12] W.H. Miller, R.M. Keenan, R.N. Willette, M.W. Lark, Identification and in vivo efficacy of small-molecule antagonists of integrin  $\alpha_v\beta_3$  (the vitronectin receptor), *Drug Discov. Today* 5 (2000) 397–408.
- [13] S.H. Tam, P.M. Sassoli, R.E. Jordan, M.T. Nakada, Abciximab (ReoPro, Chimeric 7E3 Fab) demonstrates equivalent affinity and functional blockade of glycoprotein IIb/IIIa and  $\alpha_v\beta_3$  integrins, *Circulation* 98 (1998) 1085–1091.
- [14] J. Gonzalez-Rodriguez, A.U. Acuna, M.V. Alvarez, T.M. Jovin, Rotational mobility of the fibrinogen receptor glycoprotein IIb/IIIa or integrin  $\alpha_{IIb}\beta_3$  in the plasma membrane of human platelets, *Biochemistry* 33 (1994) 266–274.
- [15] J. Yang, J. Yao, J. Chen, X.-N. Wang, T.-Y. Zhu, L.-L. Chen, P. Chu, Construction of drug screening cell model and application to new compounds inhibiting FITC-fibrinogen binding to CHO cells expressing human  $\alpha_{IIb}\beta_3$ , *Eur. J. Pharmacol.* 618 (2009) 1–8.
- [16] J.L. Seymour, W.J. Henzel, B. Nevins, J.T. Stults, R.A. Lazarus, Decorsin. A potent glycoprotein IIb-IIIa antagonist and platelet aggregation inhibitor from the leech *macrobodella decora*, *J. Mol. Biol.* 265 (1990) 10143–10147.
- [17] E.J. Topol, T.V. Byzova, E.F. Plow, Platelet GPIIb-IIIa blockers, *Lancet* 353 (1999) 227–231.
- [18] M.A. Dechantsreiter, E. Planker, B. Matha, E. Lohof, G. Holzemann, A. Jonczyk, S.L. Goodman, H. Kessler, N-Methylated cyclic RGD peptides as highly active and selective  $\alpha_v\beta_3$  integrin antagonists, *J. Med. Chem.* 42 (1999) 3033–3040.
- [19] J.A. Wendt, H. Wu, H.G. Stenmark, M.L. Boys, V.L. Downs, T.D. Penning, B.B. Chen, Y. Wang, T. Duffin, M.B. Finn, J.L. Keene, V.W. Engleman, S.K. Freeman, M.L. Hanneke, K.E. Shannon, M.A. Nickols, C.N. Steininger, M. Westlin, J.A. Klover, W. Westlin, G.A. Nickols, M.A. Russell, Synthesis of 2,5-thiazole butanoic acids as potent and selective  $\alpha_v\beta_3$  integrin receptor antagonists with improved oral pharmacokinetic properties, *Bioorg. Med. Chem. Lett.* 16 (2006) 845–849.
- [20] R.M. Keenan, W.H. Miller, C. Kwon, F.E. Ali, J.F. Callahan, R.R. Calvo, S.-M. Hwang, K.D. Kopple, C.E. Peishoff, J.M. Samanen, A.S. Wong, C.-K. Yuan, W.F. Huffman, Discovery of potent nonpeptide vitronectin receptor ( $\alpha_v\beta_3$ ) antagonists, *J. Med. Chem.* 40 (1997) 2289–2292.
- [21] D.G. Batt, J.J. Petraitis, G.C. Houghton, D.P. Modi, G.A. Cain, M.H. Corjay, S.A. Mousa, P.J. Bouchard, M.S. Forsythe, P.P. Harlow, F.A. Barbera, S.M. Spitz, R.R. Wexler, P.K. Jadhav, Disubstituted indazoles as potent antagonists of the integrin  $\alpha_v\beta_3$ , *J. Med. Chem.* 43 (1999) 41–58.
- [22] R.D. Cramer, D.E. Patterson, J.D. Bunce, Comparative molecular field analysis (CoMFA). 1. Effect of shape on binding of steroids to carrier proteins, *J. Am. Chem. Soc.* 110 (1988) 5959–5967.
- [23] G. Klebe, U. Abraham, T. Mietzner, Molecular similarity indices in a comparative analysis (CoMSIA) of drug molecules to correlate and predict their biological activity, *J. Med. Chem.* 37 (1994) 4130–4146.
- [24] M. Ishikawa, Y. Hiraiwa, D. Kubota, M. Tsushima, T. Watanabe, S. Murakami, S. Ouchi, K. Ajito, Tricyclic pharmacophore-based molecules as novel integrin  $\alpha_v\beta_3$  antagonists. Part III: Synthesis of potent antagonists with  $\alpha_v\beta_3/\alpha_{IIb}\beta_3$  dual activity and improved water solubility, *Bioorg. Med. Chem.* 14 (2006) 2131–2150.
- [25] D. Kubota, M. Ishikawa, M. Ishikawa, N. Yahata, S. Murakami, K. Fujishima, M. Kitakaze, K. Ajito, Tricyclic pharmacophore-based molecules as novel integrin  $\alpha_v\beta_3$  antagonists. Part IV: Preliminary control of  $\alpha_v\beta_3$  selectivity by meta-oriented substitution, *Bioorg. Med. Chem.* 14 (2006) 4158–4181.
- [26] Talete srl, Dragon for windows (software for molecular descriptor calculation), Version 5.4, 2006.
- [27] Y. Wang, Y. Li, J. Ding, Y. Wang, Y. Chang, Prediction of binding affinity for estrogen receptor  $\alpha$  modulators using statistical learning approaches, *Mol. Divers.* 12 (2008) 93–102.
- [28] Y. Li, Y. Wang, J. Ding, Y. Wang, Y. Chang, S. Zhang, In silico prediction of androgenic and nonandrogenic compounds using random forest, *QSAR Comb. Sci.* 28 (2008) 396–405.
- [29] X. Wang, W. Yang, X. Xu, Y. Li, Y. Wang, Studies of benzothiadiazine derivatives as hepatitis C virus NS5B polymerase inhibitors using 3D-QSAR, molecular docking and molecular dynamics, *Curr. Med. Chem.* 17 (2010) 2788–2803.

- [30] Z. Wang, Y. Li, C. Ai, Y. Wang, In silico prediction of estrogen receptor subtype binding affinity and selectivity using statistical methods and molecular docking with 2-Arylnaphthalenes and 2-Arylquinolines, *Int. J. Mol. Sci.* 11 (2010) 3434–3458.
- [31] X. Xu, W. Yang, Y. Li, Y. Wang, Discovery of estrogen receptor modulators: a review of virtual screening and SAR efforts, *Expert Opin. Drug Discov.* 5 (2010) 21–31.
- [32] J. Gasteiger, M. Marsili, Iterative partial equalization of orbital electronegativity—a rapid access to atomic charges, *Tetrahedron* 36 (1980) 3219–3228.
- [33] M. Clark, R.D. Cramer, N. Vanopdenbosch, Validation of the general-purpose tripos 5.2 force-field, *J. Comput. Chem.* 10 (1989) 982–1012.
- [34] M.D.M. AbdulHameed, A. Hamza, J. Liu, C.-G. Zhan, Combined 3D-QSAR modeling and molecular docking study on indolinone derivatives as inhibitors of 3-phosphoinositide-dependent protein kinase-1, *J. Chem. Inf. Model.* 48 (2008) 1760–1772.
- [35] J.C. Loftus, C.E. Halloran, M.H. Ginsberg, L.P. Feigen, J.A. Zablocki, J.W. Smith, The amino-terminal one-third of  $\alpha_{IIb}$  defines the ligand recognition specificity of integrin  $\alpha_{IIb}\beta_3$ , *J. Biol. Chem.* 271 (1996) 2033–2039.
- [36] D.L. French, B.S. Coller, Hematologically important mutations: glanzmann thrombasthenia, *Blood Cells Mol. Dis.* 23 (1997) 39–51.
- [37] T.A. Springer, J. Zhu, T. Xiao, Structural basis for distinctive recognition of fibrinogen  $\gamma$ C peptide by the platelet integrin  $\alpha_{IIb}\beta_3$ , *J. Cell Biol.* 182 (2008) 791–800.
- [38] J.W. Smith, D.A. Cheresh, The Arg-Gly-Asp binding domain of the vitronectin receptor. Photoaffinity cross-linking implicates amino acid residues 61–203 of the beta subunit, *J. Biol. Chem.* 263 (1988) 18726–18731.
- [39] J. Loftus, T. O'Toole, E. Plow, A. Glass, A. Frelinger 3rd, M. Ginsberg, A  $\beta_3$  integrin mutation abolishes ligand binding and alters divalent cation-dependent conformation, *Science* 249 (1990) 915–918.
- [40] B.P. Feuston, J.C. Culberson, M.E. Duggan, G.D. Hartman, C.-T. Leu, S.B. Rodan, Binding model for nonpeptide antagonists of  $\alpha_v\beta_3$  integrin, *J. Med. Chem.* 45 (2002) 5640–5648.
- [41] D.B. Kitchen, H. Decornez, J.R. Furr, J. Bajorath, Docking and scoring in virtual screening for drug discovery: methods and applications, *Nat. Rev. Drug Discov.* 3 (2004) 935–949.
- [42] D.Q. Zheng, A.S. Woodard, G. Tallini, L.R. Languino, Substrate specificity of  $\alpha_v\beta_3$  integrin-mediated cell migration and phosphatidylinositol 3-kinase/AKT pathway activation, *J. Biol. Chem.* 275 (2000) 24565–24574.
- [43] T. Kamata, A. Irie, M. Tokuhira, Y. Takada, Critical residues of integrin  $\alpha_{IIb}$  subunit for binding of  $\alpha_{IIb}\beta_3$  (glycoprotein IIb-IIIa) to fibrinogen and ligand-mimetic antibodies (PAC-1, OP-G2, and LJ-CP3), *J. Biol. Chem.* 271 (1996) 18610–18615.
- [44] I. Shindyalov, P. Bourne, Protein structure alignment by incremental combinatorial extension (CE) of the optimal path, *Protein Eng.* 11 (1998) 739–747.
- [45] J.P. Xiong, B. Mahalingham, J.L. Alonso, L.A. Borrelli, X. Rui, S. Anand, B.T. Hyman, T. Rysiok, D. Muller-Pompalla, S.L. Goodman, M.A. Arnaout, Crystal structure of the complete integrin  $\alpha_v\beta_3$  ectodomain plus an  $\alpha/\beta$  transmembrane fragment, *J. Cell Biol.* 186 (2009) 589–600.